frontiers in Soft Matter

ORIGINAL RESEARCH
published: 21 January 2022
doi: 10.3389/frsfm.2021.741996

Comparing α-Synuclein Fibrils Formed in the Absence and Presence of a Model Lipid Membrane: A Small and Wide-Angle X-Ray Scattering Study

Marija Dubackic[1]*, *Sara Linse*[2], *Emma Sparr*[1] and *Ulf Olsson*[1]

[1]Division of Physical Chemistry, Deparment of Chemistry, Lund University, Lund, Sweden, [2]Division of Biochemistry and Structural Biology, Department of Chemistry, Lund University, Lund, Sweden

Amyloid fibrils are associated with a number of different neurodegenerative diseases. Detailed knowledge of the fibril structure will be of importance in the search of therapy and may guide experiments to understand amyloid formation. In this paper we investigate the morphology of α-synuclein amyloid fibrils, associated with Parkinson's disease, formed under different conditions. In particular, we study, by means of small and wide-angle X-ray scattering, whether the presence of model lipid membranes affect the overall structure of the fibrils formed, motivated by the fact that amyloid fibrils *in vivo* are formed in a highly lipid-rich environment. Comparing fibrils formed in the presence of lipid with fibrils formed in their absence, show that the presence of lipids has no detectable effect on the fibril cross-section radius and that the characteristic β-strand repeat distance of 4.7 Å of the extended intermolecular β-sheets remains unaffected. We also show that the observed fibril radius is consistent with a fibril structure composed of two protofilaments. This indicates overall that the particular fibril structure, with their stacks of two-dimensionally folded α-synuclein molecules, represent a deep free energy minimum, not largely affected by the co-aggregation with lipids.

Keywords: amyloid fibrils, alpha-synclein, protein-lipid interactions, SAXS (small-angle X-ray scattering), WAXS (wide angle x-ray scattering), fibril structure

OPEN ACCESS

Edited by:
Nabanita Saikia,
Navajo Technical University,
United States

Reviewed by:
Maria Grazia Ortore,
Marche Polytechnic University, Italy
Reidar Lund,
University of Oslo, Norway

***Correspondence:**
Marija Dubackic
marija.dubackic@fkem1.lu.se
majuskad1@gmail.com

Specialty section:
This article was submitted to Colloids and Emulsions, a section of the journal Frontiers in Soft Matter

Received: *25 November 2021*
Accepted: *20 December 2021*
Published: *21 January 2022*

Citation:
Dubackic M, Linse S, Sparr E and Olsson U (2022) Comparing α-Synuclein Fibrils Formed in the Absence and Presence of a Model Lipid Membrane: A Small and Wide-Angle X-Ray Scattering Study. Front. Soft. Matter 1:741996. doi: 10.3389/frsfm.2021.741996

1 INTRODUCTION

Parkinson's disease (PD) is the second most common neurodegenerative disease affecting 0.3% of world's population (von Campenhausen et al., 2005). This movement disorder is marked by a loss of dopaminergic neurons in a midbrain region, *substantia nigra* (Anichtchik et al., 2000; Lehericy et al., 2014). Although symptoms of PD such as rigor, tremor and slowed motions (bradykinesia) (Fahn, 2003) may be ameliorated, the disease remains without cure. Moreover, the clinically manifested symptoms do not present themselves before 80% of dopamine signaling have been lost (Fearnley and Lees, 1991).

Multiple lines of evidence indicate that the formation of amyloid aggregates, present in so-called Lewy bodies, or the intermediate oligomeric aggregates present during the course of the aggregation process, are toxic to dopaminergic neurons and thus contributes to degeneration in PD (Bucciantini et al., 2002; Winner et al., 2011; Iyer and Claessens, 2018; Ke et al., 2020; Melo et al., 2021). A major component of Lewy bodies are fibrils formed by the protein α-synuclein, αS (Baba et al., 1998; Araki et al., 2019), a 140 amino acid-long protein abundantly expressed in neuronal cells and located in the

close proximity to lipid membranes and vesicles (O'Leary and Lee, 2019). Similar amyloid fibrils, formed by other proteins, are involved in other neurodegenerative diseases, such as Alzheimer's disease, Multiple System Atrophy, Huntington's disease and Corticobasal Degeneration.

In the search of a therapy, as well as of a better understanding of the formation of Lewy bodies and PD, a detailed knowledge of the αS fibril structure will be important. Fiber X-ray diffraction studies have confirmed the cross-β structure with β-sheets extending parallel to the fiber axis (Serpell et al., 2000). The same characteristic X-ray diffraction pattern was also recently found for Lewy bodies studied using a microbeam (Araki et al., 2019). Solid-state NMR (ss-NMR) and cryo-electron microscopy (cryo-EM) have provided detailed information on how protofilaments are built from stacking of αS molecules, being folded in two dimensions (Serpell et al., 2000; Vilar et al., 2008; Rodriguez et al., 2015; Tuttle et al., 2016; Li et al., 2018a; Li et al., 2018b; Guerrero-Ferreira et al., 2019; Pogostin et al., 2019). It has also been found that αS fibrils are composed of two left-handed intertwined protofilaments giving a fibril radius of 50 Å (Li et al., 2018b; Guerrero-Ferreira et al., 2018).

Small angle scattering of X-rays or neutrons are highly useful techniques for investigating the structure of matter on the nanometer length scale (Lindner, 2002; Glatter, 2018), including amyloid fibrils (Ricci et al., 2016). It is as such complementary to imaging techniques, like cryo-TEM (Danino, 2012; Newcomb et al., 2012), with the added advantage that it is non-destructive, and one can measure structures directly in solution. When combining with wide angle scattering, one also have access to sub-nanometer structural components, like the internal characteristic 4.7 Å spacing between β-strands in amyloid fibrils (Astbury et al., 1935; Serpell et al., 2000; Pogostin et al., 2019). In a recent study Pogostin et al. (2019) combined small and wide angle X-ray scattering, SAXS/WAXS, to investigate αS fibrils in solution as a function of pH. From SAXS it was found that the fibril cross section is approximately circular, and the 50 Å radius was confirmed. From the WAXS regime, they could also confirm the periodic 4.7 Å β-strand separation. These structural characteristics were found to be independent of pH in the range 5.5–7.5, while fibril-fibril interactions varied significantly due to alteration of the fibril net charge.

αS molecular folding and concurrent fibril formation is driven by hydrophobic interactions (Buell et al., 2012). *In vivo*, the fibril formation process occurs in a highly lipid-rich environment, and Lewy bodies are known to contain significant amounts of lipid (Shults, 2006; Stefanis, 2012; Araki et al., 2019; Fanning et al., 2020; Lashuel, 2020). These facts have motivated studies of αS-lipid interactions, involving both monomeric (Fusco et al., 2014; van Maarschalkerweerd et al., 2014; Fusco et al., 2016; Hannestad et al., 2020; Makasewicz et al., 2021), and fibrillar αS (van Rooijen et al., 2009; Hellstrand et al., 2013b; Galvagnion et al., 2019; Gaspar et al., 2021). It has been shown that monomeric αS adsorbs to anionic lipid membranes (Jao et al., 2004; Pfefferkorn et al., 2012; Hellstrand et al., 2013a; Fusco et al., 2014), and that the membrane under some conditions can have a catalytic effect on fibril formation (Galvagnion et al., 2015; Grey et al., 2015; Galvagnion, 2017; Gaspar et al., 2019). Interestingly, this adsorption appears to be a strongly cooperative process (Makasewicz et al., 2021). Several studies, performed with different systems, have also indicated that αS and lipids may form co-aggregates (Reynolds et al., 2011; Hellstrand et al., 2013b; van Maarschalkerweerd et al., 2014; Galvagnion et al., 2019; Gaspar et al., 2021). The exact nature of such aggregates still remains unclear.

Considering the lipid-rich environment that αS experiences *in vivo*, in particular in Lewy bodies (Fanning et al., 2020; Lashuel, 2020), it is important to investigate lipid effects on the fibril morphology. Therefore, we in this paper set out to investigate whether αS fibrils formed in the presence of lipid model membranes are different from the ones formed in pure buffer. Essentially following the work of Pogostin et al. (2019) who studied fibrils in pure buffer, we here present a SAXS/WAXS study of αS fibrils formed in the presence of lipid vesicles, varying the lipid concentrations and also the pH. The vesicles are composed of a mixture of phospholipids; zwitterionic POPC which is the most abundant phospholipid in the human cell membrane, and POPS which is the most common anionic phospholipid, enriched in the inner leaflet of the plasma membrane (O'Leary and Lee, 2019). All experiments were performed on mature fibrils after 14 days incubation, grown using seeds and with the wild-type αS, produced recombinantly.

2 RESULTS AND DISCUSSION

The objective of the present study is to assess the possible effects of lipids on αS fibrils. To do so, we combine small and wide-angle X-ray scattering and compare αS fibril cross-section dimensions and the periodic spacing, d_β, between β-strands in the β-sheets in fibrils formed in the absence and presence of lipid vesicles. As model lipid system we have used a mixture of 1-palmitoyl-2-oleoyl-sn-glycero-3-phosphocholine (POPC) and 1-palmitoyl-2-oleoyl-sn-glycero-3-phospho-L-serine (POPS) at a molar ratio POPC:POPS of 7:3. We have studied samples prepared at three different pH values, 6.0, 6.5 and 7.0 to modulate the overall protein net charge. In this pH range, αS, with isoelectric point at pH 4.7, has a negative net charge that increases with increasing pH (Croke et al., 2011). Furthermore, in this pH range, αS has been found to be sufficiently charged to be colloidally stable and not precipitate from solution (Pogostin et al., 2019).

Amyloid fibrils typically consist of peptide or protein molecules that are folded in two dimensions and aggregate by stacking in the third dimension through the formation of extended β-sheets. αS fibrils consist of two intertwined protofilaments (Serpell et al., 2000; Vilar et al., 2008; Rodriguez et al., 2015; Tuttle et al., 2016; Li et al., 2018a; Li et al., 2018b; Pogostin et al., 2019; Guerrero-Ferreira et al., 2019). From cryo-EM (Li et al., 2018a; Li et al., 2018b; Guerrero-Ferreira et al., 2019), solid-state NMR (Vilar et al., 2008; Tuttle et al., 2016) and spin-labeling (Chen et al., 2007) studies, it has been concluded that only the central half of the αS molecule (residues 37–99) form an ordered folded structure in the fibrils, while its C- and N- terminal regions are less ordered.

In **Figure 1A** we present the SAXS pattern, I(q), of αS fibrils formed at pH 6.0 in the absence of lipids at a protein concentration of 280 μM, and a PDB structure, obtained from cryo-EM (Li et al., 2018b) is shown in **Figure 1B**. In order to

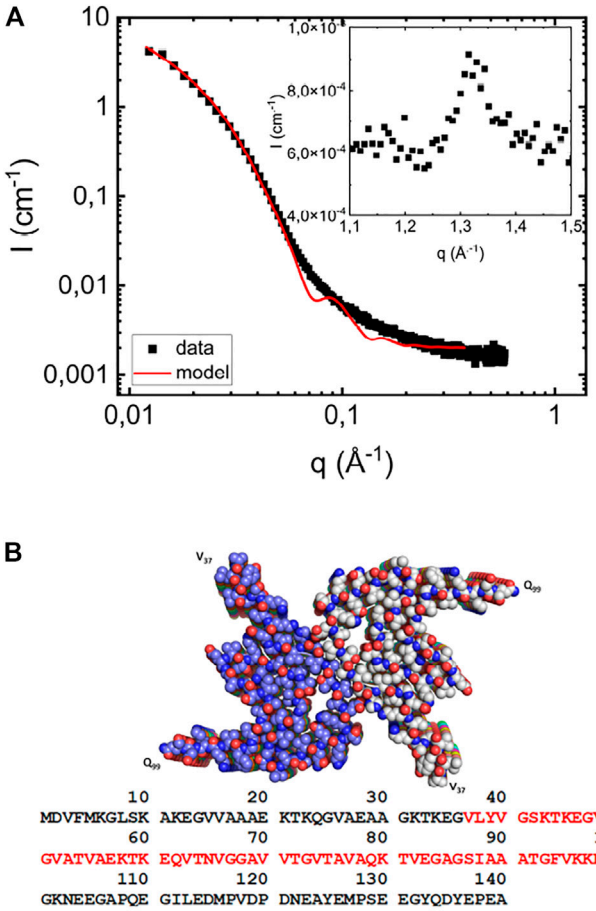

FIGURE 1 | (A) Scattering profile of fibrils formed in the absence of vesicles at a protein concentration of 280 μM at pH 6.0 (filled black squares). The solid red line is the simulated scattering pattern based on the elliptical cylinder model. As an inset, the wide-angle diffraction pattern, with a peak at $q = 1.3\ \AA^{-1}$, is shown. **(B)** PDB structure (6A6B) of the 2D-folded protein obtained from cryo-EM (Li et al., 2018b) (top). The PDB structure includes only residues composing the fibril core, αS (37–99), and we show the two protofilaments in different colors. In the amino acid sequence (bottom), residues composing the core are shown in red.

estimate the fibril cross section dimension, we have modeled the fibrils as elliptical cylinders, and a calculated model scattering curve is shown as a solid line in **Figure 1A**. The fibrils are very long, having an overall length $L \gg q_{\min}^{-1}$, where $q_{\min}$ is the minimum q-value accessible in the experimental q-range, and not measurable in the present experiments. Because of the large L, the fibril form factor can be factorized into a product of the overall length and cross-section contributions, respectively (Glatter and Kratky, 1983). With $L \gg q_{\min}^{-1}$ the model scattered intensity can be written as

$$I(q) = \frac{C}{q} P_c(q), \tag{1}$$

where $P_c(q)$ is the normalized two-dimensional cross-section form factor, and the parameter C is given by

$$C = \pi \Delta\rho^2 \phi_p \frac{V_p}{L}. \tag{2}$$

Here, $\Delta\rho = \rho_p - \rho_b$ is the scattering length density difference between protein (p) and buffer (b), ϕ_p is the fibril (protein) volume fraction, and V_p/L is the protein volume per unit length in the fibrils. As the fibrils are composed of two protofilaments, we have $V_p/L = 2v_p/d_\beta$, where $v_p = 17\ \mathrm{nm}^3$ is the αS molecular volume, assuming a mass density of $1.4\ g/cm^3$, and $d_\beta = 4.7$ Å is the periodic repeating β-strand separation in the β-sheets. The X-ray scattering length densities are given by $\rho_p = 13\ 10^{10}\ cm^{-2}$ and $\rho_b = 9.5\ 10^{10}\ cm^{-2}$, respectively. The normalized cross-section form factor of an elliptical cylinder can be written as

$$P_c(q) = \frac{2}{\pi} \int_0^{\pi/2} d\varphi \left(\frac{J_1(qr)}{qr} \right)^2 \tag{3}$$

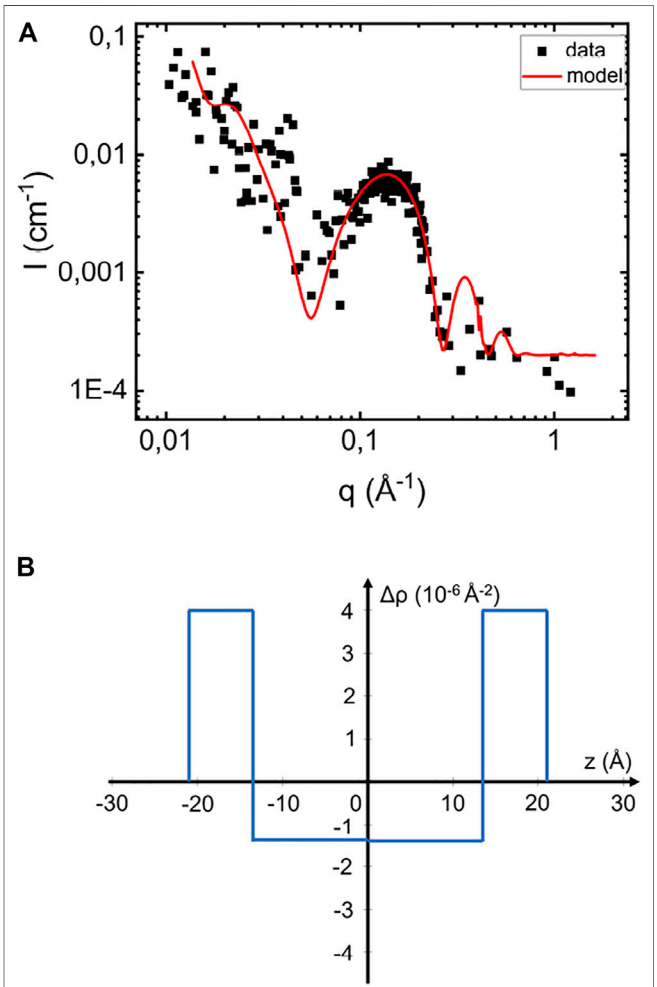

FIGURE 2 | (A) Scattering profile of pure vesicles suspension at pH 6.6 and 2.1 mM and the simulated scattering pattern based on the core-multi-shell model (red line). **(B)** Illustration of the scattering length density difference variation across the bilayer in the normal direction.

where $J_1(x)$ is the first order Bessel function and $r = ((\text{asin}(\varphi)^2 + (b\cos\varphi)^2)^{1/2}$ is an effective radius that varies with the polar angle φ. **Eq. 3** is obtained from the full elliptical cross-section cylinder model given for example in ref. (Pedersen, 1997), after performing the factorization (**Eq. 1**). An elliptical cross-section, with minor semi-axis a = 5 nm and major semi-axis b = 10 nm, together with a protein concentration of 250 μM, is found to describe the SAXS pattern satisfactorily, and is shown as the solid line in **Figure 1A**. An additional analysis of V_p/L (or mass per unit length) is presented in the SI, confirming a fibril structure of two protofilaments.

At higher q-values, $q > 0.5$ Å^{-1}, $I(q)$ levels off to a constant value of approximately 1.7 $10^{-3} cm^{-1}$. This is considered in the model as a constant "background" term arising from electron density variations inside the fibrils. As an inset in **Figure 1A** we also present a part of the WAXS pattern, which shows a peak at q = 1.3 Å^{-1}. This characteristic peak corresponds to a periodic repeat distance of d_β = 4.7 Å, and is the repeating β-strand separation in the β-sheets (Serpell et al., 2000). This repeat distance is commonly observed in fibrils formed by other proteins, for example Amyloid-β (Serpell, 2000), as well as for short peptides (Kuczera et al., 2020; Narayanan et al., 2021). The same β-strand repeat distance is also found in fibrils of NACore [αS (68–78)], an 11 residue central segment of αS (Rodriguez et al., 2015; Pallbo et al., 2019).

Phospholipids, with their relatively high electron density polar headgroups and low electron density acyl chains, have an average X-ray scattering length density very close to that of water (Kucerka et al., 2011). Consequently, such membranes scatter only weakly at lower $q \ll 1/\delta$, where δ is the overall bilayer thickness. In **Figure 2A** we present SAXS pattern of a POPC/POPS vesicle samples at a lipid concentration of 2.1mM, and pH 6.0. The POPC:POPS molar ratio is 7:3. The vesicle hydrodynamic radius, R_H, as obtained from DLS is 180 ± 40 Å. As can be seen, the low q scattering is very weak, however a broad maximum is visible around q = 0.15 Å^{-1}, reporting on the scattering length density profile across the bilayer. Following Pallbo et al. (2020), we have modeled the vesicle scattering using a core-multi-shell model composed of an aqueous core and three shells describing the bilayer. The inner and outer shells, each 7.5 Å thick, represent the inner and outer headgroup layer, respectively, and the middle shell, 27 Å thick, represents the acyl-chain region. The corresponding radial scattering length density profile of the model is shown in **Figure 2B**, with the acyl chains scattering length density equal to 8.1 10^{10} cm^{-2} and the one of the headgroup layer equal to 13.5 10^{10} cm^{-2}. Adjusting model to the data, we obtained ϕ = 4.5 10^{-3}.

The scattered intensity from the vesicle dispersion can be written as $I_v(q) = \phi_L V_v \Delta\rho_L^2 < P_v(q) >$, where ϕ_L is the lipid volume fraction, V_v is the bilayer volume in a vesicle, $\Delta\rho_L$ is the overall scattering length density difference between lipid and solvent, and $< P_v(q) >$ is the average vesicle form factor, taking into account size polydispersity. For the three-shell model, $P_v(q)$ can be written as

$$P_v(q) = \frac{1}{M}\left(\rho_1 V(R_1)F(1,R_1) + \sum_{i=2}^{4}(\rho_i - \rho_{i-1})V(R_i)F(q,R_i)\right)^2 \quad (4)$$

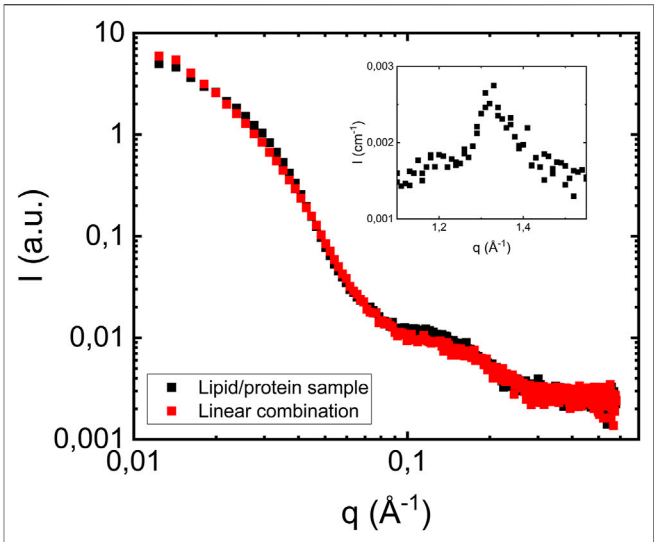

FIGURE 3 | Scattering profile of a sample where fibrils were formed in the presence of vesicles at pH 6.0 (filled black squares). The protein concentration is 280 μM, and lipid to protein molar ratio is equal to 7.5. Red squares show a linear combination of scattering profiles of fibrils formed in the absence of vesicles (**Figure 1A**) and vesicles scattering profiles (**Figure 2A**). As an inset the wide-angle diffraction pattern from the L/P = 7.5, with a peak at q = 1.3 Å^{-1}, is shown.

where $F(q,R_i) = 3(\sin(q,R_i) - qR_i\cos(q,R_i))/(qR_i)^3$ is the form factor amplitude of a sphere with radius R_i, $M = \rho_1 V(R_1) + \sum_{i=2}^{3} V(R_i)(\rho_i - \rho_{i-1})$ is the total scattering length of the core-shell particle, $V(R_i) = 4\pi R_i^3/3$ is the volume of the sphere with radius R_i, and ρ_i is the scattering length density of the ith shell (Pedersen, 1997). i = 1 corresponds to the outer headgroup shell. Hence, R1 corresponds to the outer vesicle radius and R4 is the radius of the inner aqueous core. A cartoon illustrating the different radii is shown in **Supplementary Figure S1** of the SI.

Shown in **Figure 2A** as solid line is a simulated scattering curve that is modeling the main feature of the scattering pattern, the form factor hump around q = 0.15 Å^{-1}, which is reflecting the particular electron density variation across the bilayer. As can be seen, the model accounts well for this feature. Based on the R_H = 180 Å obtained from DLS, the model assumes $< R4 >$ = 140 Å, and a polydispersity of 30%, corresponding to the relative standard deviation of a Gaussian size distribution. Thus $< R1 >$ = 182 Å, which is consistent with R_H obtained from DLS. However, we note that SAXS intensity is very low at lower q-values and thus rather insensitive to the vesicle radius. The same data shown in **Figures 1A**, **2B**, including error bars for the intensity are presented in SI.

Having established how the lipid membranes scatter in the investigated q-range, we now turn to the case when fibrils are formed in the presence of lipid vesicles. In **Figure 3** we show the SAXS pattern from a sample with 280 = μM αS and 2.1 mM of lipid, corresponding to a lipid to protein molar ratio of 7.5 (L/P = 7.5). The pattern is very similar to that of the fibril formed in the absence of lipids (**Figure 1A**), but with the additional broad hump around q = 0.15 Å^{-1}, corresponding to scattering from the lipid bilayer. As expected, this hump is the only visible

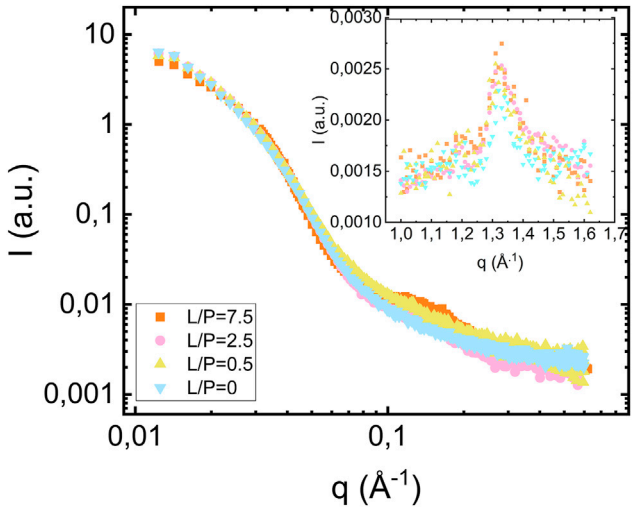

FIGURE 4 | Scattering from fibrils formed in the presence of vesicles at different lipid concentrations [L/P = 7.5 (orange square), L/P = 2.5 (pink circles), L/P = 0.5 (yellow triangles pointing up)] and in the absence of vesicles (blue triangle pointing down) at pH 6.0. The protein concentration is equal to 280 μM. The inset shows the wide-angle diffraction region with diffraction peak at q = 1.3 Å^{-1}.

contribution from the lipids to the scattering pattern. The red symbols are showing the linear combination of scattering profiles obtained from fibrils formed in the absence of vesicles and scattering profiles of pure vesicle dispersion. We note that the fibril concentration was higher in the presence of lipid, and the pure fibril scattering from **Figure 1A** was multiplied with 1.4 in order to overlap with the scattering from the L/P = 7.5 sample. The lipid contribution, on the other hand was not scaled.

As can be seen, a linear combination describes the data well. This is a key result that implies that the presence of POPC/POPS vesicles have no, or at least no detectable effects on the αS fibril cross-section dimension nor the extended intermolecular β-sheet structure. Also, the fact that we do not see any decrease in the bilayer concentration implies that most of the lipids, if not all, remain in bilayer aggregates with the same dimension as in the pure vesicle sample.

We also investigated samples composed of fibrils prepared at lower lipid concentrations. In **Figure 4** we compare the scattering profiles obtained when αS fibrils are formed at pH 6.0 at protein concentration of 280 μM in the presence of lipid vesicles at three different lipid concentrations, corresponding to lipid-to-protein molar ratios L/P = 0, 2.5 and 7.5. In addition, we also show the scattering for the case of protein alone (L/P = 0). As can be seen, the fibril scattering is essentially identical in these four cases. The bilayer scattering is only clearly visible for the highest lipid concentration, L/P = 7.5. For the two lower lipid concentrations, L/P = 0.5 and 2.5, the lipid contribution is not enough to be visible. The insert in **Figure 4** shows the wide-angle regime data for the different L/P and all samples show the characteristic diffraction peak at q = 1.3 Å^{-1}, corresponding to the d_β = 4.7 Å periodic β-strand stacking parallel to the fibril axis, which is unaffected by the presence of lipids.

For the highest lipid-to-protein ratio, L/P = 7.5, we also investigated samples prepared at pH 6.5 and 7.0. The SAXS patterns from the samples at different pH values are compared in **Figure 5**. As can be seen, both the fibril and bilayer scattering is essentially identical in these three cases. As an insert of **Figure 5**, we show the wide-angle diffraction pattern with an identical diffraction peak at q = 1.3 $\mathring{A}^{-1}$ in all cases.

In this study, we varied pH in the range 6.0–7.0, without observing any pH effects. While physiological pH generally is considered to be 7.4, there are weakly acidic cellular compartments like lysosomes and endosomes (Demaurex, 2002; Hu et al., 2015) that may be relevant for αS fibril formation.

The formation of protein-lipid co-aggregates were shown for similar αS-lipid systems, DOPC:DOPS 7:3 at a slightly lower pH = 5.5 (Hellstrand et al., 2013b) and DMPC and DLPS at pH = 6.5 (Galvagnion et al., 2019) by means of solid-state NMR. There are also several other reports on the formation of lipid-protein co-aggregates. Both in the case of the early stage of aggregation, involving membrane disruption and protein oligomer formation (Fusco et al., 2014; van Maarschalkerweerd et al., 2014; Fusco et al., 2016; Hannestad et al., 2020), and in the case of mature fibrils (van Rooijen et al., 2009; Grey et al., 2011; Gaspar et al., 2021). However, the very nature of co-aggregation is not fully clear in the case of mature fibrils. Authors are unable to tell if the association of lipids and fibrils is integrated, with lipids being intercalating the β-strands or otherwise incorporated in the fibril structure, or external, where bilayers are adsorbed onto the fibril surface (Hellstrand et al., 2013b; Galvagnion et al., 2019). Possibly, it mainly involves an attractive interaction between pure αS fibril and pure lipid membrane, leaving the internal fibril structure unperturbed. In the present study, we do not observe mixing of lipid and protein on the molecular length scale

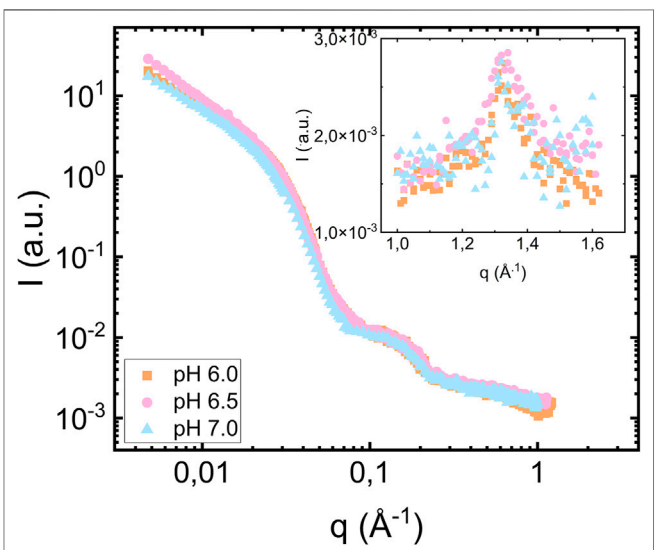

FIGURE 5 | Scattering from fibrils formed in the presence of vesicles at pH 6.0 (orange square), 6.5 (pink circles) and 7.0 (blue triangles pointing up). The protein concentration is equal to 280 μM and the lipid to protein ratio is equal to 7.5. The inset shows the wide-angle diffraction region with diffraction peak at q = 1.3 Å^{-1}.

but we do not exclude the possibility that intact fibrils may associate with bilayer membranes in such a manner that the fibrils become coated with bilayers or have vesicles adsorbed along their length.

In the samples shown in our study, we are using seeds to accelerate fibril formation and therefore the catalytic effect of model membranes is probably negligible. The exact nucleation condition is probably not important for whether one observes an uptake of lipid into the fibrils (co-aggregation) or not. The reason is because the nucleation events are very few compared to the so-called elongation (growth) events, *id est*, the addition of protein monomers at the ends of existing fibrils. αS fibrils are many micrometers long, also in the presence of lipids, and typically consist of the order of 10^4 αS molecules. A critical nucleus on the hand is much smaller and may contain perhaps 10 or perhaps even 100 molecules. This implies that if there would be a significant amount of lipid incorporated into the formed fibrils, then this will happen rather during the growth phase than during the nucleation phase.

By means of cryo-TEM, Hellstrand and co-workers showed that fibrils associate differently in clusters when they are formed in the presence and absence of lipids, as well as that there are no free excess lipid vesicles in the case of L/P = 1 and the presence of deformed vesicles at higher lipid to protein ratios (Hellstrand et al., 2013b). This tells that lipids interact with the formed fibrils and that the vesicles collapse during fibril formation. In the present study, we do not see a change in the fibril cross section radius when the fibrils are formed in the presence of lipid. We note, however, that the molecular volume of αS is approximately 15 times larger than the volume of a lipid molecule. Hence, if all the lipid molecules, in the case of L/P = 0.5 would be mixed into the fibrils, this would only correspond to a minor increase in fibril volume that could be difficult to detect in the SAXS pattern. We also note that the protein forms a highly specific and densely folded structure in fibrils (Tuttle et al., 2016; Li et al., 2018a; Guerrero-Ferreira et al., 2019) as seen in **Figure 1B**. This dense folding is driven by hydrophobic interactions and reduces water contact with the many hydrophobic residues in the central NAC region of the αS molecule.

How αS monomers, oligomers and fibrils interact with lipid membranes is an important question that has been addressed in a number of studies. It is well established that αS monomers adsorb to anionic membranes with the N-terminal region, and undergo a conformational change from disordered to a high degree of α-helix structure (Jao et al., 2004; Fusco et al., 2014). Anionic lipid membranes may also catalyze fibril formation by acting a site for heterogeneous nucleation (Galvagnion et al., 2015; Grey et al., 2015; Galvagnion, 2017; Gaspar et al., 2019). A major question also concerns whether formed fibrils, or intermediate oligomers, disrupt vesicle structures, which can be a possible cause of toxicity (van Maarschalkerweerd et al., 2014). Lewy bodies, a hallmark of Parkinson's disease, are intracellular inclusions rich in αS fibrils, but also containing significant amounts of lipid and organelles (Shults, 2006; Stefanis, 2012; Araki et al., 2019; Fanning et al., 2020; Lashuel, 2020). The mechanism of Lewy body formation is not known, but possibly are result of significant attractive interactions between αS fibrils and lipid membranes. αS fibrils have been found to show attractive, presumably hydrophobic, fibril-fibril interactions (Semerdzhiev et al., 2018; Pogostin et al., 2019) and it is possible that there can be similar attractive fibril-membrane interactions. However, fibrils were shown to bind to lipid DOPC/DOPS (molar ratio 7/3) giant uni-lamellar vesicle (GUV) membranes but not to pure DOPC membranes, indicating the importance of electrostatic interactions, similar to the case of monomer interaction with membranes (Grey et al., 2011).

The present study adds additional important information to the ongoing debate on αS-lipid interaction. We have shown that αS fibrils formed in the presence of POPC/POPS (7/3) lipid vesicles have the same cross-section dimension, and two intertwined protofilaments, as fibrils formed in the absence of lipid. Also, the β-sheet stacking, with the characteristic 4.7 Å periodicity, is unaffected. This indicates that the stacking of the two-dimensionally folded αS molecules and the two-protofilament fibril structure represent a robust protein aggregate structure, not largely affected by the presence of lipids. The 4.7 Å periodicity was also recently observed in a scanning WAXS experiment on Lewy bodies, using a microbeam (Araki et al., 2019).

In the present study we do not observe any swelling of the fibrils nor the formation of a different fibril structure, when αS fibrils are formed in the presence of POPC/POPS model membranes. We cannot exclude the possibility of small amounts lipid molecules being incorporated into the fibrils, to an extent that is not affecting the fibril radius. However, if so they are most likely present in the outer layer of the fibrils that are believed to be less ordered. In the central core of the fibrils the protein is densely folded (Guerrero-Ferreira et al., 2020) and most likely less prone to mix with lipid. For the highest lipid concentration (L/P = 7.5) the scattering contribution from lipid bilayers were observed in the SAXS pattern with an intensity that indicated that essentially all lipid molecules remained in the bilayer structures.

3 MATERIALS AND METHODS

3.1 α-Synuclein

Human αS (molar mass, M_w = 14.4 kg mol^{-1}) was expressed in *Escherichia coli* and purified using heat treatment, ion exchange and gel filtration chromatography, as described previously in Grey et al. (2011). Prior to incubation with lipid vesicles, αS was purified by size exclusion chromatography (SEC) in phosphate buffer, using a Superdex 75 column (GE Healthcare). The protein concentration was measured using the integrated absorbance at 280 nm of the collected fraction from the SEC chromatogram assuming a molar extinction coefficient 5.960 $M^{-1}cm^{-1}$. αS monomers collected from SEC were lyophilized to obtain high concentration required for scattering experiments.

3.2 Preparation of Vesicles

1-palmitoyl-2-oleoyl-sn-glycero-3-phosphocholine (POPC) and 1-palmitoyl-2-oleoyl-sn-glycero-3-phospho-L-serine (POPS)

were purchased from Avanti Lipids and used as received. In all experiments, a molar ratio POPC:POPS = 7:3 was used. Vesicles were prepared by first dissolving appropriate amounts of lipid in the chloroform methanol mixture (chloroform to methanol 3:1 volume ratio). The solvent was evaporated underneath a stream of N_2 gas, and the newly formed lipid film was dried in vacuum oven over night. The lipids were then dispersed in phosphate buffer at pH 6.0, 6.5 and 7.0. Solutions were sonicated on ice for 15 min (10 s on/off duty and 70% amplitude) using Sonics, Vibra-Cell tip sonicator. The vesicle dispersion was centrifuged at 13 ,000 rpm for 15 min in order to pellet metal residues from the sonicator tip and the supernatant was used as the final vesicle dispersion. The size of vesicles was estimated by means of dynamic light scattering (DLS) (Zetasizer Nano ZS from Malvern) and their radius was found to be on average 180 ± 40 Å.

3.3 Preparation of Fibrils

The lyophilized powder was resuspended in filtered (0.2 μm) H_2O. Seeds, i.e., preformed αS fibrils, were added to a concentration corresponding to 5% of the total αS concentration in monomer units. Finally, a lipid vesicle solution was added. In the end, the final concentration of αS monomers was equal to 280 μM. The samples were prepared with three lipid concentration: 140 μM (lipid/protein ratio L/P = 0.5), 700 μM (L/P = 2.5) and 2.1 mM (L/P = 7.5). All samples were incubated in Axygen low-binding Eppendorf tubes at 37°C for 14 days under quiescent conditions.

3.4 Small-Angle X-Ray Scattering

X-ray scattering experiments were performed on a Saxslab Ganesha pinhole instrument JJ X-ray System APS (JJ X-ray, Hoersholm, Denmark) with an X-ray microsource (Xenocs, Sassenage, France) and a two-dimensional 300 k Pilatus detector (Dectris Ltd., Baden-Daettwil, Switzerland). Three sample-to-detector distances were used and the X-ray wavelength, λ, was 1.54 Å. The two-dimensional scattering pattern was always isotropic (circularly symmetric) and was therefore radially averaged to obtain the one-dimensional scattering function, I(q), where $q = \frac{4\pi}{\lambda} \sin \frac{\theta}{2}$ is the magnitude of the scattering vector, θ being the scattering angle. Absolute scaling of the scattered intensity was performed by using water as a calibration standard. Scattering from the buffer measured in the same capillary as the sample was subtracted. Data were modeled using the SasView software (www.sasview.org).

DATA AVAILABILITY STATEMENT

The raw data supporting the conclusions of this article will be made available by the authors, without undue reservation.

AUTHOR CONTRIBUTIONS

MD, ES, SL, and UO conceived and designed the study. MD conducted all experiments. MD wrote the article with input from all co-authors.

FUNDING

This work was supported by Swedish Foundation for Strategic Research through the national Graduate School SwedNessESS (GSn15-0008), the Swedish Research Council VR (SL 2015-00143) and the Knut and Alice Wallenberg Foundation grant (ES, SL, UO 2016.0074).

ACKNOWLEDGMENTS

This work benefited from the use of the SasView application, originally developed under NSF award DMR-0520547. SasView contains code developed with funding from the European Union's Horizon 2020 research and innovation program under the SINE2020 project, grant agreement No. 654000.

SUPPLEMENTARY MATERIAL

The Supplementary Material for this article can be found online at: https://www.frontiersin.org/articles/10.3389/frsfm.2021.741996/full#supplementary-material

REFERENCES

Anichtchik, O. V., Rinne, J. O., Kalimo, H., and Panula, P. (2000). An Altered Histaminergic Innervation of the Substantia Nigra in Parkinson's Disease. *Exp. Neurol.* 163, 20–30. doi:10.1006/exnr.2000.7362

Araki, K., Yagi, N., Aoyama, K., Choong, C.-J., Hayakawa, H., Fujimura, H., et al. (2019). Parkinson's Disease Is a Type of Amyloidosis Featuring Accumulation of Amyloid Fibrils of α-synuclein. *Proc. Natl. Acad. Sci. USA* 116, 17963–17969. doi:10.1073/pnas.1906124116

Astbury, W. T., Dickinson, S., and Bailey, K. (1935). The X-ray Interpretation of Denaturation and the Structure of the Seed Globulins. *Biochem. J.* 29, 2351–2360. doi:10.1042/bj0292351

Baba, M., Nakajo, S., Tu, P. H., Tomita, T., Nakaya, K., Lee, V. M., et al. (1998). Aggregation of Alpha-Synuclein in Lewy Bodies of Sporadic Parkinson's Disease and Dementia with Lewy Bodies. *Am. J. Pathol.* 152, 879–884.

Bucciantini, M., Giannoni, E., Chiti, F., Baroni, F., Formigli, L., Zurdo, J., et al. (2002). Inherent Toxicity of Aggregates Implies a Common Mechanism for Protein Misfolding Diseases. *Nature* 416, 507–511. doi:10.1038/416507a

Buell, A. K., Dhulesia, A., White, D. A., Knowles, T. P. J., Dobson, C. M., and Welland, M. E. (2012). Detailed Analysis of the Energy Barriers for Amyloid Fibril Growth. *Angew. Chem. Int. Ed.* 51, 5247–5251. doi:10.1002/anie.201108040

Chen, M., Margittai, M., Chen, J., and Langen, R. (2007). Investigation of α-Synuclein Fibril Structure by Site-Directed Spin Labeling. *J. Biol. Chem.* 282, 24970–24979. doi:10.1074/jbc.M700368200

Croke, R. L., Patil, S. M., Quevreaux, J., Kendall, D. A., and Alexandrescu, A. T. (2011). NMR Determination of pKa Values in α-synuclein. *Protein Sci.* 20, 256–269. doi:10.1002/pro.556

Demaurex, N. (2002). pH Homeostasis of Cellular Organelles. *Physiology* 17 (1), 1–5. doi:10.1016/j.cocis.2012.10.003

Danino, D. (2012). Cryo-tem of Soft Molecular Assemblies. *Curr. Opin. Colloid Interf. Sci.* 17, 316–329. doi:10.1016/j.cocis.2012.10.003

Fahn, S. (2003). Description of Parkinson's Disease as a Clinical Syndrome. *Ann. N Y Acad. Sci.* 991, 1–14. doi:10.1111/j.1749-6632.2003.tb07458.x

Fanning, S., Selkoe, D., and Dettmer, U. (2020). Parkinson's Disease: Proteinopathy or Lipidopathy? *Npj Parkinsons Dis.* 6. doi:10.1038/s41531-019-0103-7

Fearnley, J. M., and Lees, A. J. (1991). Ageing and Parkinson's Disease: Substantia Nigra Regional Selectivity. *Brain* 114, 2283–2301. doi:10.1093/brain/114.5.2283

Fusco, G., De Simone, A., Gopinath, T., Vostrikov, V., Vendruscolo, M., Dobson, C. M., et al. (2014). Direct Observation of the Three Regions in α-synuclein that Determine its Membrane-Bound Behaviour. *Nat. Commun.* 5. doi:10.1038/ncomms4827

Fusco, G., Pape, T., Stephens, A. D., Mahou, P., Costa, A. R., Kaminski, C. F., et al. (2016). Structural Basis of Synaptic Vesicle Assembly Promoted by α-synuclein. *Nat. Commun.* 7, 12563. doi:10.1038/ncomms12563

Galvagnion, C., Buell, A. K., Meisl, G., Michaels, T. C. T., Vendruscolo, M., Knowles, T. P. J., et al. (2015). Lipid Vesicles Trigger α-synuclein Aggregation by Stimulating Primary Nucleation. *Nat. Chem. Biol.* 11, 229–234. doi:10.1038/nchembio.1750

Galvagnion, C. (2017). The Role of Lipids Interacting with α-Synuclein in the Pathogenesis of Parkinson's Disease. *Jpd* 7, 433–450. doi:10.3233/JPD-171103

Galvagnion, C., Topgaard, D., Makasewicz, K., Buell, A. K., Linse, S., Sparr, E., et al. (2019). Lipid Dynamics and Phase Transition within α-Synuclein Amyloid Fibrils. *J. Phys. Chem. Lett.* 10, 7872–7877. doi:10.1021/acs.jpclett.9b03005

Gaspar, R., Idini, I., Carlström, G., Linse, S., and Sparr, E. (2021). Transient Lipid-Protein Structures and Selective Ganglioside Uptake during α-Synuclein-Lipid Co-aggregation. *Front. Cel Dev. Biol.* 9, 266. doi:10.3389/fcell.2021.622764

Gaspar, R., Pallbo, J., Weininger, U., Linse, S., and Sparr, E. (2018). Ganglioside Lipids Accelerate α-synuclein Amyloid Formation. *Biochim. Biophys. Acta (Bba) - Proteins Proteomics* 1866, 1062–1072. doi:10.1016/j.bbapap.2018.07.004

Glatter, O. (2018). *Scattering Methods and Their Application in Colloid and Interface Science*. Elsevier.

Glatter, O., and Kratky, O. (1983). *Small-angle X-ray Scattering*. London, NY: Academic Press. doi:10.1002/actp.1985.010360520

Grey, M., Dunning, C. J., Gaspar, R., Grey, C., Brundin, P., Sparr, E., et al. (2015). Acceleration of α-Synuclein Aggregation by Exosomes. *J. Biol. Chem.* 290, 2969–2982. doi:10.1074/jbc.M114.585703

Grey, M., Linse, S., Nilsson, H., Brundin, P., and Sparr, E. (2011). Membrane Interaction of α-Synuclein in Different Aggregation States. *J. Parkinson's Dis.* 1, 359–371. doi:10.3233/JPD-2011-11067

Guerrero-Ferreira, R., Taylor, N. M., Arteni, A. A., Kumari, P., Mona, D., Ringler, P., et al. (2019). Two New Polymorphic Structures of Human Full-Length Alpha-Synuclein Fibrils Solved by Cryo-Electron Microscopy. *eLife* 8, e48907. doi:10.7554/eLife.489010.7554/eLife.48907

Guerrero-Ferreira, R., Taylor, N. M., Mona, D., Ringler, P., Lauer, M. E., Riek, R., et al. (2018). Cryo-em Structure of Alpha-Synuclein Fibrils. *eLife* 7, e36402. doi:10.7554/eLife.36402.001

Guerrero-Ferreira, R., Kovacik, L., Ni, D., and Stahlberg, H. (2020). New Insights on the Structure of Alpha-Synuclein Fibrils Using Cryo-Electron Microscopy. *Curr. Opin. Neurobiol.* 61, 89–95. doi:10.1016/j.conb.2020.01.014

Hannestad, J. K., Rocha, S., Agnarsson, B., Zhdanov, V. P., Wittung-Stafshede, P., and Höök, F. (2020). Single-vesicle Imaging Reveals Lipid-Selective and Stepwise Membrane Disruption by Monomeric α-synuclein. *Proc. Natl. Acad. Sci. USA* 117, 14178–14186. doi:10.1073/pnas.1914670117

Hellstrand, E., Grey, M., Ainalem, M.-L., Ankner, J., Forsyth, V. T., Fragneto, G., et al. (2013a). Adsorption of α-Synuclein to Supported Lipid Bilayers: Positioning and Role of Electrostatics. *ACS Chem. Neurosci.* 4, 1339–1351. doi:10.1021/cn400066t

Hellstrand, E., Nowacka, A., Topgaard, D., Linse, S., and Sparr, E. (2013b). Membrane Lipid Co-aggregation with α-Synuclein Fibrils. *PLoS ONE* 8, e77235. doi:10.1371/journal.pone.0077235

Hu, Y. B., Dammer, E. B., Ren, R. J., and Wang, G. (2015). The Endosomal-Lysosomal System: From Acidification and Cargo Sorting to Neurodegeneration. *Transl. Neurodegener.* 4 (1), 18. doi:10.1186/s40035-015-0041-1

Iyer, A., and Claessens, M. M. A. E. (2019). Disruptive Membrane Interactions of Alpha-Synuclein Aggregates. *Biochim. Biophys. Acta (Bba) - Proteins Proteomics* 1867, 468–482. doi:10.1016/j.bbapap.2018.10.006

Jao, C. C., Der-Sarkissian, A., Chen, J., and Langen, R. (2004). From the Cover: Structure of Membrane-Bound -synuclein Studied by Site-Directed Spin Labeling. *Proc. Natl. Acad. Sci.* 101, 8331–8336. doi:10.1073/pnas.0400553101

Ke, P. C., Zhou, R., Serpell, L. C., Riek, R., Knowles, T. P. J., LashuelGazit, H. A. H. A. L., et al. (2020). Half a century of Amyloids: Past, Present and Future. *Chem. Soc. Rev.* 49, 5473–5509. doi:10.1039/C9CS00199A

Kučerka, N., Nieh, M.-P., and Katsaras, J. (2011). Fluid Phase Lipid Areas and Bilayer Thicknesses of Commonly Used Phosphatidylcholines as a Function of Temperature. *Biochim. Biophys. Acta (Bba) - Biomembranes* 1808, 2761–2771. doi:10.1016/j.bbamem.2011.07.022

Kuczera, S., Rüter, A., Roger, K., and Olsson, U. (2020). Two Dimensional Oblique Molecular Packing within a Model Peptide Ribbon Aggregate. *ChemPhysChem* 21, 1519–1523. doi:10.1002/cphc.201901126

Lashuel, H. A. (2020). Do lewy Bodies Contain Alpha-Synuclein Fibrils? and Does it Matter? a Brief History and Critical Analysis of Recent Reports. *Neurobiol. Dis.* 141, 104876. doi:10.1016/j.nbd.2020.104876

Lehéricy, S., Bardinet, E., Poupon, C., Vidailhet, M., and François, C. (2014). 7 Tesla Magnetic Resonance Imaging: A Closer Look at Substantia Nigra Anatomy in Parkinson's Disease. *Mov Disord.* 29, 1574–1581. doi:10.1002/mds.26043

Li, B., Ge, P., Murray, K. A., Sheth, P., Zhang, M., Nair, G., et al. (2018a). Cryo-EM of Full-Length α-synuclein Reveals Fibril Polymorphs with a Common Structural Kernel. *Nat. Commun.* 9. doi:10.1038/s41467-018-05971-2

Li, Y., Zhao, C., Luo, F., Liu, Z., Gui, X., Luo, Z., et al. (2018b). Amyloid Fibril Structure of α-synuclein Determined by Cryo-Electron Microscopy. *Cell Res* 28, 897–903. doi:10.1038/s41422-018-0075-x

Lindner, P., and Zemb, T. (2002). *Neutron, X-Rays and Light Scattering Methods Applied to Soft Condensed Matter*. Amsterdam: Elsevier.

Makasewicz, K., Wennmalm, S., Stenqvist, B., Fornasier, M., Andersson, A., Jönsson, P., et al. (2021). Cooperativity of α-Synuclein Binding to Lipid Membranes. *ACS Chem. Neurosci.* 12, 2099–2109. doi:10.1021/acschemneuro.1c00006

Melo, F., Caballero, L., Zamorano, E., Ventura, N., Navarro, C., Doll, I., et al. (2021). The Cytotoxic Effect of α-Synuclein Aggregates. *ChemPhysChem* 22, 526–532. doi:10.1002/cphc.202000831

Narayanan, T., Rüter, A., and Olsson, U. (2021). SAXS/WAXS Investigation of Amyloid-B(16-22) Peptide Nanotubes. *Front. Bioeng. Biotechnol.* 9, 654349. doi:10.3389/fbioe.2021.654349

Newcomb, C. J., Moyer, T. J., Lee, S. S., and Stupp, S. I. (2012). Advances in Cryogenic Transmission Electron Microscopy for the Characterization of Dynamic Self-Assembling Nanostructures. *Curr. Opin. Colloid Interf. Sci.* 17, 350–359. doi:10.1016/j.cocis.2012.09.004

O'Leary, E., and Lee, J. (2019). Interplay between α-synuclein Amyloid Formation and Membrane Structure. *Biochim. Biophys. Acta - Proteins Proteomics* 1867, 483–491. doi:10.1016/j.bbapap.2015.08.009

Pallbo, J., Imai, M., Gentile, L., Takata, S.-I., Olsson, U., and Sparr, E. (2020). Nacore Amyloid Formation in the Presence of Phospholipids. *Front. Physiol.* 11, 1708. doi:10.3389/fphys.2020.592117

Pallbo, J., Sparr, E., and Olsson, U. (2019). Aggregation Behavior of the Amyloid Model Peptide NACore. *Quart. Rev. Biophys.* 52, 1–10. doi:10.1017/S0033583519000039

Pedersen, J. S. (1997). Analysis of Small-Angle Scattering Data from Colloids and Polymer Solutions: Modeling and Least-Squares Fitting. *Adv. Colloid Interf. Sci.* 70, 171–210. doi:10.1016/S0001-8686(97)00312-6

Pfefferkorn, C. M., Heinrich, F., Sodt, A. J., Maltsev, A. S., Pastor, R. W., and Lee, J. C. (2012). Depth of α-Synuclein in a Bilayer Determined by Fluorescence, Neutron Reflectometry, and Computation. *Biophysical J.* 102, 613–621. doi:10.1016/j.bpj.2011.12.051

Pogostin, B. H., Linse, S., and Olsson, U. (2019). Fibril Charge Affects α-Synuclein Hydrogel Rheological Properties. *Langmuir* 35, 16536–16544. doi:10.1021/acs.langmuir.9b02516

Reynolds, N. P., Soragni, A., Rabe, M., Verdes, D., Liverani, E., Handschin, S., et al. (2011). Mechanism of Membrane Interaction and Disruption by α-Synuclein. *J. Am. Chem. Soc.* 133, 19366–19375. doi:10.1021/bm500937p10.1021/ja2029848

Ricci, C., Spinozzi, F., Mariani, P., and Grazia Ortore, M. (2016). Protein Amyloidogenesis Investigated by Small Angle Scattering. *Cpd* 22, 3937–3949. doi:10.2174/1381612822666160519113237

Rodriguez, J. A., Ivanova, M. I., Sawaya, M. R., Cascio, D., Reyes, F. E., Shi, D., et al. (2015). Structure of the Toxic Core of α-synuclein from Invisible Crystals. *Nature* 525, 486–490. doi:10.1038/nature15368

Semerdzhiev, S. A., Lindhoud, S., Stefanovic, A., Subramaniam, V., van der Schoot, P., and Claessens, M. M. A. E. (2018). Hydrophobic-Interaction-Induced Stiffening of α -Synuclein Fibril Networks. *Phys. Rev. Lett.* 120, 208102. doi:10.1103/PhysRevLett.120.208102

Serpell, L. C. (2000). Alzheimer's Amyloid Fibrils: Structure and Assembly. *Biochim. Biophys. Acta (Bba) - Mol. Basis Dis.* 1502, 16–30. doi:10.1016/s0925-4439(00)00029-6

Serpell, L. C., Berriman, J., Jakes, R., Goedert, M., and Crowther, R. A. (2000). Fiber Diffraction of Synthetic Alpha -synuclein Filaments Shows Amyloid-like Cross-Beta Conformation. *Proc. Natl. Acad. Sci.* 97, 4897–4902. doi:10.1073/pnas.97.9.4897

Shults, C. W. (2006). Lewy Bodies. *Proc. Natl. Acad. Sci.* 103, 1661–1668. doi:10.1073/pnas.0509567103

Stefanis, L. (2012). -Synuclein in Parkinson's Disease. *Cold Spring Harbor Perspect. Med.* 2, a009399. doi:10.1101/cshperspect.a009399

Tuttle, M. D., Comellas, G., Nieuwkoop, A. J., Covell, D. J., Berthold, D. A., Kloepper, K. D., et al. (2016). Solid-state NMR Structure of a Pathogenic Fibril of Full-Length Human α-synuclein. *Nat. Struct. Mol. Biol.* 23, 409–415. doi:10.1038/nsmb.3194

van Maarschalkerweerd, A., Vetri, V., Langkilde, A. E., Foderà, V., and Vestergaard, B. (2014). Protein/Lipid Coaggregates Are Formed during α-Synuclein-Induced Disruption of Lipid Bilayers. *Biomacromolecules* 15, 3643–3654. doi:10.1021/bm500937p

van Rooijen, B. D., Claessens, M. M. A. E., and Subramaniam, V. (2009). Lipid Bilayer Disruption by Oligomeric α-synuclein Depends on Bilayer Charge and Accessibility of the Hydrophobic Core. *Biochim. Biophys. Acta (Bba) - Biomembranes* 1788, 1271–1278. doi:10.1016/j.bbamem.2009.03.010

Vilar, M., Chou, H.-T., Luhrs, T., Maji, S. K., Riek-Loher, D., Verel, R., et al. (2008). The Fold of -synuclein Fibrils. *Proc. Natl. Acad. Sci.* 105, 8637–8642. doi:10.1073/pnas.0712179105

von Campenhausen, S., Bornschein, B., Wick, R., Bötzel, K., Sampaio, C., Poewe, W., et al. (2005). Prevalence and Incidence of Parkinson's Disease in Europe. *Eur. Neuropsychopharmacol.* 15, 473–490. doi:10.1016/j.euroneuro.2005.04.007

Winner, B., Jappelli, R., Maji, S. K., Desplats, P. A., Boyer, L., Aigner, S., et al. (2011). *In Vivo* demonstration that -synuclein Oligomers Are Toxic. *Proc. Natl. Acad. Sci.* 108, 4194–4199. doi:10.1073/pnas.1100976108

Conflict of Interest: The authors declare that the research was conducted in the absence of any commercial or financial relationships that could be construed as a potential conflict of interest.

Publisher's Note: All claims expressed in this article are solely those of the authors and do not necessarily represent those of their affiliated organizations, or those of the publisher, the editors and the reviewers. Any product that may be evaluated in this article, or claim that may be made by its manufacturer, is not guaranteed or endorsed by the publisher.